PAPER

Check for updates

Porous calcium silicate bioactive material–alginate composite for bone regeneration†

Shital S. Shendage,[a] Kranti Kachare,[a] Kajal Gaikwad,[b] Shivaji Kashte[b] and Anil Vithal Ghule [ID] *[a]

Bone tissue engineering aims to address bone-related problems that arise from trauma, infection, tumors, and surgery. Polymer and calcium silicate bioactive material (BM) based composites are commonly preferred as potential materials for bone treatment. However, the polymer has low bioactivity, thus, the current work aims to prepare a composite scaffold based on BM–sodium alginate (Alg) by varying the Alg percentage to optimize the porous nature of the composite. Primarily, the BM was synthesized by a simple precipitation method using rice husk and eggshell as the precursors of silica and calcium, while the BM–Alg composite was prepared by a facile cross-linking approach. The BM–Alg composite was studied using XRD, FTIR, SEM, and BET techniques. Further, an *in vitro* bioactivity study was performed in simulated body fluid (SBF) which shows hydroxyapatite formation. The *in vitro* haemolysis study displayed less than 5% haemolysis. Subsequently, the angiogenesis study was carried out using the *ex ovo* CAM model which reveals enhanced neovascularization. The MG-63 cells were used to study the biocompatibility, and they displayed a non-toxic nature at a concentration of 10 mg mL^{-1}. Further, the *in vivo* biocompatibility results also reveal its non-toxic nature. Thus, the BM–Alg composite acts as a potential biocompatible material for bone tissue engineering applications.

1. Introduction

The bone tissue engineering field has developed potential techniques to regenerate damaged/diseased bones injured by tumors, trauma, and bone diseases (osteoporosis, osteomyelitis). Metal implants, allograft, and autograft techniques have been used for the treatment of damaged bone by replacing it with an artificial bone graft (scaffold).[1] However, the disadvantages related to these techniques include the release of ions into blood, re-surgery over a certain period, matching of blood group, donor site morbidity, and cost.[2] Due to the scarcity of these techniques, the synthesis of biocompatible bone scaffolds has recently gained much attention in orthopedics. Several biocompatible scaffolds made from organic (polymers) and inorganic (ceramics) materials have been used for bone regeneration applications.[3]

The polymeric scaffold made from sodium alginate (Alg), chitosan, collagen, polylactic acid (PLA) and polycaprolactone (PCL) are used for bone regeneration because of their flexibility, biocompatibility, biodegradability, and mechanical properties.[4] Specifically, Alg is widely used as a competitive material in the medical field due to its biocompatible, biodegradable, and hydrophilic nature. In addition, Alg not only mimics the properties of the extracellular matrix (ECM) but also achieves a balance between mechanical strength, porosity, and degradation.[5] The Alg is a linear polymer composed of D-mannuronate (M) and L-guluronate (G) monomers which are covalently bonded. However, biopolymers alone lack bioactivity and osteoconductivity. To overcome these limitations, the polymers were combined with an inorganic material such as calcium silicate bioactive material (BM), hydroxyapatite (HAp), wollastonite, β-tricalcium phosphate (β-TCP) due to their inherent bioactivity and osteoconductivity.[3] Among them, BM is considered a preferred material over other inorganic materials because of their bonding with soft and hard tissues.[6-8] Since the remarkable findings by Prof. Hench, BMs have been widely utilized as bone substitute materials due to their essential properties such as biocompatibility, osteoinductivity, and osteoconductivity, which are crucial for successful bone regeneration.[9] Additionally, BM also promotes osteoblast cell differentiation, neovascularization, and osteogenesis, and further contributes to the overall success of bone regeneration

[a]Department of Chemistry, Green Nanotechnology Laboratory, Shivaji University, Kolhapur 416004, India. E-mail: avg_chem@unishivaji.ac.in

[b]Department of Stem Cell and Regenerative Medicine, Centre for Interdisciplinary Research, D. Y. Patil Education Society (Institution Deemed to Be University), Kolhapur, India

† Electronic supplementary information (ESI) available: Fig. S1 TGA thermogram of 1% BM–Alg (red curve), 3% BM–Alg (black curve), and 5% BM–Alg (purple curve) composite. Fig. S2 BET (surface area analysis) and BJH (pore size distribution) of (a) 1% (red curve), (b) 3% (black curve), (c) 5% (purple curve) BM–Alg, and (d) 1% BM–Alg 700 °C (blue curve). Fig. S3 (a) XPS survey spectrum and (b) TEM images of 1% BM–Alg 700 °C. Fig. S4 Plausible mechanism and nature of bonding in the composite. Table S1. Lethality assay using brine shrimp. See DOI: https://doi.org/10.1039/d4ra02763a

processes.[10] Modification by introducing BM with Alg is one of the options to improve the biological properties of the composite.[3,11]

In addition, designing a scaffold with properties similar to those of natural bone plays a crucial role in eliciting a favorable biological response. Therefore, the synthesis of a composite with the balance between porosity, degradation, bioactivity, angiogenesis, and mechanical properties acts as a potential candidate for bone regeneration. This facilitates cell attachment, proliferation, and differentiation, which is further essential for successful tissue regeneration.[2] Among all, porosity plays a major role because the porous scaffolds help to enhance the degradation rate by exchanging the ions with the surrounding medium. In addition, implantation of porous graft *in vivo* shows neovascularization which further continues to new bone tissue formation.[12] In addition, the porous nature increases cell migration, vascularisation, and nutrient and oxygen transport.[13] Further, the porous graft also acts as an advantageous platform for drug delivery.[14]

Literature reports reveal that BM–Alg composite scaffolds with varying BM compositions have been explored to take advantage of their unique properties. The synthesis of strontium and zinc-containing BM–Alg composite scaffold is reported using the freeze-drying method to make it biocompatible, bioactive, and porous for bone tissue engineering applications.[15] Similarly, the preparation of porous BM–Alg scaffold is reported by freeze-drying as a bone substitute material.[16] The BM–Alg composite scaffold prepared from 3D printing has also been explored to study the controlled drug release behavior required for bone tissue engineering.[17] BM have also been reported to be synthesized using chemical precursors,[15,16] while the composite scaffolds were synthesized using advanced techniques.[14,18] However, with the motivation to develop greener approaches, considering the cost of the chemical precursors and limited availability of advanced techniques,[19] the development of a cost-effective scaffold using a simple processing method for bone treatment is the need of the time.

Thus, in the present study, novel 70S30C BM was synthesized by using recycled biowaste materials, rice husk (silica source), and eggshell (calcium source), respectively, by simple precipitation method. Further, to achieve porosity, vascularization, and degradation, the 70S30C BM was composited with Alg by simple crosslinking. Further, to enhance the porosity, in the present study, the BM–Alg composite was calcined with the expectation that the organics in Alg would decompose to form carbonaceous material creating pores which also form the basis of our investigation. In addition, there are quite a few literature reports available on the synthesis of BM–alginate composite, however, most of the synthesis of BM–alginate composites are done using commercially available chemical precursors and biowaste materials. However, our motivation was to synthesize the BM–alginate composites using a greener approach and to explore the possibility of synthesizing the same using recycled agricultural bio-waste materials which poses significant challenges in recycling them leading to environmental pollution and health concerns if discarded untreated. Furthermore, recycling bio-waste materials rather than just discarding them contributes to environmental protection and prevents the destruction of natural habitats contributing to Sustainable Development Goals (SDGs). Subsequently, the as-prepared BM–Alg composite was subjected to BET, XRD, FTIR, and SEM analysis, and the results were compared with the calcined BM–Alg composite. The *in vitro* bioactivity, degradation, haemolysis, angiogenesis, and *in vitro* and *in vivo* biocompatibility study of the BM–Alg composite were examined.

2. Experimental

2.1 Preparation of silica and calcium oxide

The rice husk (collected from a rice mill, Gokul Shirgaon, Kolhapur, India) was used as a source of silica. The rice husk was cleaned with hydrochloric acid (0.5 N–HCl, Sigma-Aldrich). Then the rice husk was washed and neutralized with distilled water (D.W.) followed by drying and calcination (600 °C for 4 h). Meanwhile, the eggshells (obtained from the local market) were used as a source of calcium which was cleaned, dried, crushed in fine powder, and then calcined at 900 °C for 2 h to obtain calcium oxide.

2.2 Preparation of BM–Alg composite

The 70S30C BM was prepared by simple precipitation method using rice husk and eggshell as a source of silica and calcium. In brief, 0.3 g calcium oxide was added to the ammonium hydroxide solution (NH₄OH, Sigma-Aldrich) and stirred for the formation of calcium hydroxide. Meanwhile, the SiO₂ (0.7 g) powder was added to 2 N sodium hydroxide (NaOH, Sigma-Aldrich) with heating and stirring conditions for the formation of sodium silicate. Further, sodium silicate was added to the calcium hydroxide solution with continuous stirring and heating for 30 min. Then, the solution was sonicated for 30 min and kept overnight for aging. The resultant precipitate was washed, filtered, dried, and calcined at 700 °C for 2 h in an air atmosphere. Further, the synthesized BM powder was used to make the BM–Alg composite by simple cross-linking. Firstly, the 1% Alg solution was prepared by dissolving 1 g of Alg in 100 mL of D.W. Then 1 g of BM powder was added to the above-prepared Alg solution under continuous stirring for 1 h. After that, 1% calcium chloride solution (CaCl₂) (1 g CaCl₂ was dissolved in 100 mL D.W.) was added to the above solution with continuous stirring for 1 h to enhance the crosslinking. The prepared solution was kept overnight for homogenization. The obtained 1% BM–Alg composite solution was washed with D.W. and dried in an oven and used for further characterization. A similar process was followed to prepare 3 and 5% BM–Alg composite. Further, the 1% BM–Alg, 3% BM–Alg, and 5% BM–Alg composite were investigated for their porous nature and further to enhance the porous nature of the composite, the optimized composite was calcined at 700 °C (BM–Alg 700 °C).

2.3 Characterization of BM–Alg composite

The phase and crystal structure present in BM–Alg and BM–Alg 700 °C composites were studied by X-ray diffraction (XRD) using Bruker D8-Phaser diffractometer (Cu Kα₁ radiation, 1.54 Å wavelength, 40 kV, 40 mA). The crystallite size of the BM–Alg composite was calculated using the Debye Scherrer eqn (1);

$$D = \frac{0.9\lambda}{\beta \cos \theta} \qquad (1)$$

where λ is monochromatic X-ray wavelength, β is full-width half maxima-FWHM, and θ is the angle of diffraction. Further, the inter-molecular bonding between BM and Alg was characterized by Fourier transform infrared spectroscopy (FTIR) using Bruker Alpha-100508 spectrometer in transmittance mode (4000–400 cm^{-1} wavenumber). The surface morphology was analyzed by scanning electron microscopy (SEM-JEOL, JSM-IT200). The composite of BM with Alg was studied by thermogravimetric analysis (TGA-TA Instrumentation, SDT Q 600). The porous nature in terms of surface area and pore size of the BM–Alg composite was evaluated by using Brunauer–Emmett–Teller (BET-NOVA1000e Quantachrome, USA) and Barret–Joyner–Halenda (BJH) analyses. The chemical composition present in the synthesized material was analyzed by the X-ray photoelectron spectroscopy (XPS-JEOL Japan JPS 9030) analysis, whereas, morphology of the material was studied by transmission electron microscopy (TEM-JEOL). Further, the *in vitro* bioactivity was performed to analyze HAp formation on the BM–Alg composite.

2.4 *In vitro* bioactivity

The *in vitro* bioactivity of the synthesized composite was evaluated in a simulated body fluid (SBF) solution. SBF was prepared according to the Kokubo method.[20] The BM–Alg composite pellets (13 mm wide and 1 mm height having 0.3 g weight) were prepared by Hydraulic pellet press method and immersed in SBF solution (7.43 pH) and kept in a shaking incubator at 37 °C for 3, 7, and 14 days. Then the pellets were removed, washed, and dried. Finally, pellets were characterized using XRD, FTIR, and SEM analysis to determine the HAp growth. Further, a degradation study was performed.

2.5 Degradation study

The degradation or weight loss percentage of the pellets (13 mm wide and 1 mm height having 0.3 g pellet weight) was examined in SBF solution. The pellets were weighed before immersion (WB) and then immersed in SBF solution (30 mL) at 37 °C for 3, 7, and 14 days. Then, the pellets were removed from SBF, washed, and dried in an oven. The weight of the sample after (WA) immersion in SBF was noted and the weight loss percentage was calculated using eqn (2);

$$\text{Percentage weight loss} = \frac{\text{WB} - \text{WA}}{\text{WB}} \times 100 \qquad (2)$$

Then, the haemolysis study was carried out to evaluate the haemocompatibility of the BM–Alg composite using human blood *in vitro*.

2.6 Haemolysis study

The collected blood from the human donor was centrifuged for 15 min at 3000 rpm. After that in the settled blood pellet, the 2 mL phosphate-buffered saline (PBS) was mixed. In the meantime, sample (10 mg) and normal saline (10 mL) were added in falcon tubes and tubes were placed in a water bath at 37 °C for 30 min. Then, the 200 μL blood was added to it and again placed in a water bath having 37 °C temperature for 2 h followed by centrifugation for 15 min at 3000 rpm. After that, the absorbance of the supernatant solution was measured at 540 nm using a UV-visible spectrophotometer. The haemolysis percentage of the BM–Alg sample was estimated using eqn (3);

$$\text{Percentage of haemolysis} =$$

$$\frac{\text{O.D. of sample} - \text{O.D positive control}}{\text{O.D. positive control} - \text{O.D of negative control}} \times 100 \qquad (3)$$

Further, the angiogenesis study was performed using *ex ovo* Chorioallantoic Membrane Assay (CAM) assay.

2.7 Angiogenesis study

The fertilized eggs (zero-day) were brought from an egg hatchery, Kolhapur, Maharashtra, India. The eggs were disinfected using alcohol (70%) and placed in an incubator at 37 °C for 3 days for the development of primary blood vessels. The eggs were removed from the incubator and further, the CAM assay process was conducted in a laminar hood. To produce free space in the egg, 4–5 mL albumen was removed from the narrow side of the egg using a syringe and then the hole was closed using cello tape. From the blunt side of the egg, the shell was cracked (2–3 cm area) and 0.01 g of BM–Alg powder was placed near the embryo. The opened eggshell was closed with cello tape and parafilm tape to avoid bacterial infection and the eggs were then incubated in an incubator at 37 °C. The growth of the blood vessels was observed and compared with the control after 24, 48, and 96 h, while the control is CAM without the addition of the sample.[21] Further, to support these CAM results the biocompatibility study was performed using MG-63 cells.

2.8 *In vitro* biocompatibility assay

2.8.1 Lethality assay using brine shrimp. The lethality assay using brine shrimp was examined in the present study according to Meyer *et al.*[22] Initially, brine shrimp eggs were hatched in artificial seawater and incubated for 48 h, to get phototropic nauplii (first larval stage) and used in further experiments. The brine shrimp were nourished with a diet of Brewer's yeast (6 mg L^{-1}). For the experimental setup, 0.5 mL of sample solution (10 μg, 500 μg, 1000 μg) was introduced into a vial containing 4.5 mL of brine solution along with 10 shrimp. The control vial consists of 4.5 mL of artificial seawater and a mixture of 0.5 mL of artificial seawater and 0.2% dimethyl sulfoxide (DMSO) solution. These vials were exposed to a lighted area. After 24 h of incubation period, the survived shrimps were counted using a $3 \times$ magnifying glass, and the percentage of mortality was calculated using an eqn (4);

$$\text{Percentage death} = \frac{\text{total nauplii} - \text{alive nauplii}}{\text{total nauplii}} \times 100 \qquad (4)$$

2.8.2 MTT assay. The MTT assay was conducted to evaluate the impact of synthesized samples on osteosarcoma MG-63 cells. MG-63 cells (1×10^{-4} cells mL^{-1}) were initially cultured in Dulbecco's modified Eagle's medium (DMEM) at 37 °C for 24 h within a CO_2 atmosphere. Subsequently, 70 μL of cells per well were seeded in culture media, and in the culture media 100 μL of sample solution (2.5, 5, 10 mg mL^{-1}) were added to separate wells in 96 well plates. All sample plates were incubated at 37 °C in a CO_2 atmosphere for 24 h in triplicate. After incubation, 20 μL of MTT solution was employed to assess viable cells by measuring the optical density of the samples at a wavelength of 570 nm. The control well consisted of a solution of dimethyl sulfoxide (DMSO) and MG-63 cells. The percentage inhibition was calculated using eqn (5), and subsequently, the percentage cell viability was determined using eqn (6);

$$\text{Percentage inhibition} = \frac{\text{control} - \text{test}}{\text{control}} \times 100 \qquad (5)$$

$$\text{Percentage cell viability} = 100 - \text{percent inhibition} \qquad (6)$$

Further, to support the biocompatibility study, the *in vivo* subcutaneous study was performed.

2.9 *In vivo* biocompatibility

The *in vivo* biocompatibility study was conducted in collaboration with the Animal Ethics Committee at D. Y. Patil Medical College Kolhapur (Approval No. 6/IAEC/2017). To assess the biocompatibility of the BM–Alg and BM–Alg 700 °C, the rats aged 8–10 weeks and weighing approximately 250 g were used in triplicates. The study was followed according to ethical principles and animal care guidelines, encompassing proper anesthesia and surgical procedures. Anesthesia was induced using ketamine (100 mg kg^{-1}) and xylazine (5 mg kg^{-1}) injections. Subsequently, a ~1 cm incision was made, and skin pockets were formed in the subcutaneous region of the rat. The control was considered without the addition of a sample in the rat skin pocket whereas, for the sample autoclaved powdered disc pellet was implanted into the skin pocket, followed by suturing with nylon thread. The study was executed for 14 days, and *in vivo* biocompatibility was checked and the photographs were taken. The interaction between the sample and tissue was assessed in terms of histology.

2.9.1 Histology. The tissue from the implanted area was harvested and preserved in neutral buffered formalin (NBF-10%). Then, the tissue was dehydrated and xylene was used for clearing, followed by the preparation of paraffin wax blocks. The processed tissue sections were then stained using hematoxylin and eosin (H&E). Photographs of the stained tissue sections were captured using a compound microscope (Leica DM 750), which was equipped with a camera. This allowed for a detailed examination of the histological features and interactions between the implanted material and the surrounding tissue.

2.10 Statistical analysis

The experiments were repeated three times and presented as mean ± standard deviation. The comparison between the groups was studied by one-way ANOVA and the significance was considered $p < 0.05$ (*$p \le 0.05$, **$p \le 0.01$, ***$p \le 0.001$) with the Dunnet comparison test.

The present study was performed in strict accordance with ethical principles and animal care guidelines and approved by Shivaji University, Kolhapur and D. Y. Patil Medical College Kolhapur, India (Approval No. 6/IAEC/2017).

3. Results and discussions

The BM was synthesized using recycled rice husk and eggshells as a source of silica and calcium using the precipitation method without the use of acid, binder, and surfactant. The BM was composited with Alg having 1, 3, and 5% of Alg and denoted as 1%, 3%, and 5% BM–Alg. Further, the porous nature was enhanced by calcining 1% BM–Alg at 700 °C. The XRD, FTIR, and SEM analyses were used to examine the structural and physicochemical properties of the synthesized composites.

The formation of the composite of BM with Alg was confirmed by the TGA analysis. Fig. S1† shows the TGA thermogram of the 1%, 3%, and 5% BM–Alg composite. The TGA thermogram of 1%, 3%, and 5% BM–Alg composite shows almost similar trend in which, the first step weight loss (12, 8, and 12%), second step weight loss (19, 28, and 31%), and third step weight loss (8, 9, and 9%) could be attributed to the loss of moisture, decomposition of organics, formation of carbonaceous material and oxidation of carbonaceous material, respectively. It is interesting to note that after the oxidation of the carbonaceous matter, the remaining inorganic matter accounts for the BM, thus, 1, 3, and 5% BM–Alg composite consist of 61, 55, and 48% BM, respectively. Further, it was observed that the 1% BM–Alg consists of more residual content than 3% BM–Alg, than 5% BM–Alg. It could be due to the composition of Alg used during the synthesis of the BM–Alg composite. Specifically, during the synthesis of 1% BM–Alg composite, 1 g Alg was used whereas, during the synthesis of 3% BM–Alg and 5% BM–Alg composite 3 and 5 g Alg was used. This means that the 1% BM–Alg contains less amount of Alg consequently it shows less decomposition as compared with the 3% BM–Alg, than 5% BM–Alg.

Fig. 1 shows the BET and BJH results for 1%, 3%, and 5% BM–Alg composite. The 70S30C BM showed a 74.65 m^2 g^{-1} surface area,[23] whereas, the 1%, 3%, and 5% BM–Alg composite showed 275.79, 62.35, and 27.36 m^2 g^{-1} surface area (Fig. 1a) with 19, 17, and 21 nm average pore size (Fig. 1b) that revealed the mesoporous nature of the composite. The 1%, 3%, and 5% BM–Alg composite displayed Type IV isotherm and H3 hysteresis loop. It was observed that the addition of Alg in BM leads to an increase in surface area of 1% BM–Alg composite due to crosslinking between BM and Alg. The surface area was found to be decreased with an increase in Alg percentage because the polymers help to provide mechanical strength.[24] The literature report reveals that the surface area of the mesoporous BG was found to be 187.2 m^2 g^{-1} and the composite was used for bone regeneration application.[25] It is obvious that the higher surface area helps to transport nutrients and ions during the bone healing process and provides more HAp formation.[26] In

addition, higher surface area enhances cell attachment, and proliferation, and helps to facilitate the delivery of the growth factor and drug molecules.[8] According to the results and literature, the 1% BM–Alg composite was selected for further study due to higher surface area as compared with the 3%, and 5% BM–Alg composite. Further, to probe for the possibility of an increase in the surface area by decomposing the Alg from the 1% BM–Alg composite, in the present study the 1% BM–Alg composite was calcined at 700 °C for 2 h (1% BM–Alg 700 °C). The result shows 298.67 m^2 g^{-1} surface area (Fig. 1a) with 2.4 nm average pore size (Fig. 1b). It was observed that the calcination of 1% BM–Alg at 700 °C helps to enhance the surface area when compared with the as-synthesized BM (74.65 m^2 g^{-1}). For a clear understanding, the separate BET and BJH plots of 1%, 3%, 5% BM–Alg, and 1% BM–Alg 700 °C composite were plotted as shown in Fig. S3.†

The XRD study was performed to detect the phase and crystal structure present in 1% BM–Alg and 1% BM–Alg 700 °C and the results were compared with the 70S30C BM. Fig. 1c shows an XRD pattern of 70S30C BM, 1% BM–Alg, and 1% BM–Alg 700 °C composite. The 70S30C BM, 1% BM–Alg, and 1% BM–Alg 700 °C showed crystalline nature with ~35, ~14, and ~10 nm crystallite size, and all diffraction peaks were matched with JCPDS-027-0088. It was observed that the 1% BM–Alg composite showed a small hump between 8 and 20° due to the presence of Alg.[27] Whereas, the hump is not seen in the 1% BM–Alg 700 °C composite due to calcination at 700 °C. In addition, the synthesized samples show a crystalline nature due to the formation of sodium calcium silicate crystal phase.[28,29] The bonding between BM and Alg was analyzed using FTIR data. Fig. 1d demonstrates FTIR spectra for 70S30C BM, 1% BM–Alg, and 1% BM–Alg 700 °C. The 70S30C BM showed Si–O–Si stretching (symmetric and asymmetric) at ~638, 1021, and 1074 cm^{-1}, Si–O–Si bending at ~450 cm^{-1}, and Si–O–NBO non-bridging oxygen at ~897, ~930 cm^{-1}.[23] The 1% BM–Alg 700 °C
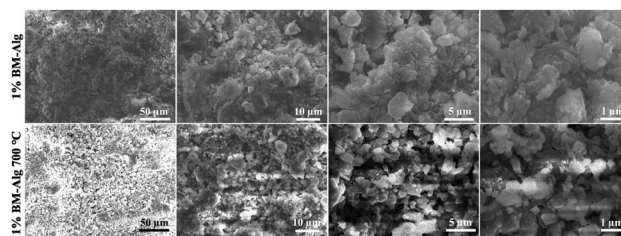

Fig. 2 SEM images of 1% BM–Alg and 1% BM–Alg 700 °C composite at different magnification.

shows peaks for Si–O–Si stretching, bending, and non-bridging oxygen. Whereas, an intense peak observed in 1% BM–Alg 700 °C at ~1474 was due to calcination. In addition, to analyze the crosslinking between BM, Alg, and $CaCl_2$, peaks present in 1% BM–Alg composite were interpreted. The Alg consists of mannuronic acid and glucuronic acid.[8,30] The 1% BM–Alg composite shows a peak at ~1424 cm^{-1} attributed to the –COO^- group. Whereas, ~1608 and ~1251 are detected for glucuronic acid and mannuronic acid.[8] The peaks at ~3450 (–OH) and ~1635 cm^{-1} (H–O–H) present in all samples were associated with the hydroxy group. Further, the surface morphology of 1% BM–Alg and 1% BM–Alg 700 °C composite were analyzed by SEM analysis as shown in Fig. 2. The 1% BM–Alg composite shows compacted particles (Fig. 2) whereas, 1% BM–Alg 700 °C (Fig. 2) demonstrates uneven surface morphology with free particles. The change in morphology between 1% BM–Alg and 1% BM–Alg 700 °C composite was observed due to calcination. It was observed that, charging effect leads to blurred images of the samples despite epitaxial coating to minimize charging effect with the understanding that the thicker conductive coating would affect the observed morphology. It is interesting to note that the calcination of the composite results in the decomposition of alginate in the composite and it was intended to enhance the porosity by creating channels for ion transport. The respective insets in the images show magnified SEM images. Further, the chemical composition in the 1% BM–Alg 700 °C was studied by XPS analysis. Fig. S3a† shows the XPS spectrum of the synthesized material. The XPS survey spectrum of 1% BM–Alg 700 °C (Fig. S3†) shows peaks related to C1s, O1s, Ca2p, and Si2p elements having binding energies of 285 eV, 533 eV, 349 eV, and 104 eV respectively.[31] Further, the TEM study for 1% BM–Alg 700 °C was carried out as shown in Fig. S3b.† It is observed that the 1% BM–Alg 700 °C particles show combination of spherical and rod like morphology with ~76 nm size. The earlier literature reports also reveal the spherical particles with the formation of rod like structures.[32] In addition to this, the plausible mechanism between BM and Alg was depicted as shown in Fig. S4.† The sodium alginate consists of carboxyl and hydroxyl groups. The functional groups present on polymer leads to crosslinking through hydrogen, covalent, and ionic bonding and then the addition of BM further helps for crosslinking due to presence of calcium, sodium ions attached to silicate network. After confirmation of composite formation, the *in vitro* pH study was performed in SBF solution to monitor the HAp growth by measuring the change in pH values observed
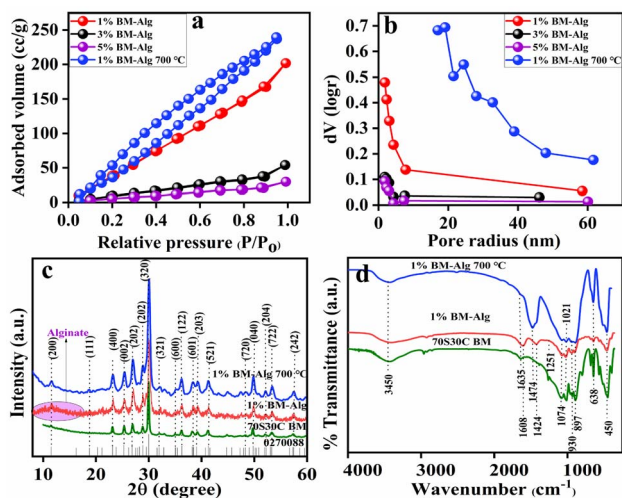

Fig. 1 (a) BET (surface area analysis). (b) BJH (pore size distribution) of 1% (red curve), 3% (black curve), 5% (purple curve) BM–Alg, and 1% BM–Alg 700 °C (blue curve). (c) XRD and (d) FTIR analysis of 70S30C BM, 1% BM–Alg, and 1% BM–Alg 700 °C composite.
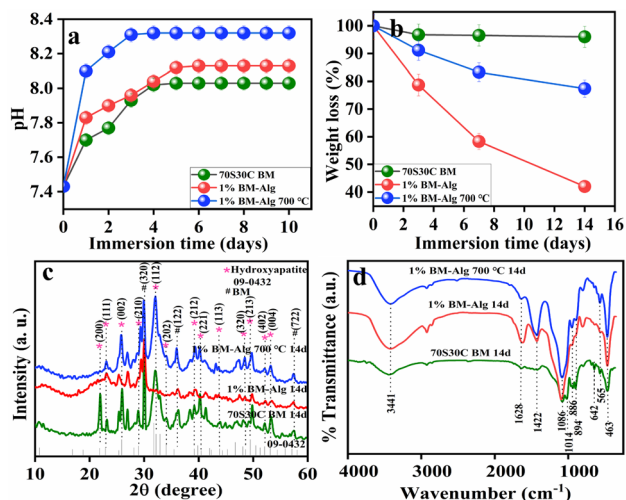
Fig. 3 (a) Changes observed in pH values up to 10 days of immersion of 70S30C BM, 1% BM–Alg, and 1% BM–Alg 700 °C composite in SBF as a function of time. (b) Weight loss percentage of 70S30C BM, 1% BM–Alg, and 1% BM–Alg 700 °C pellet after 3, 7, and 14 days of immersion in SBF. (c) Representative XRD and (d) FTIR spectra of 70S30C BM, 1% BM–Alg, and 1% BM–Alg 700 °C after 14 days of *in vitro* bioactivity study.

due to the release of ions from the BM–Alg composite in SBF solution.

Fig. 3 displays the pH study for 70S30C BM, 1% BM–Alg, and 1% BM–Alg 700 °C composite after immersion in SBF for up to 10 days. The pH of the solutions was checked after 24 h up to 10 days. The changes in pH values were associated with HAp formation by ion exchange between the sample surface and the SBF solution. The 70S30C BM, 1% BM–Alg, and 1% BM–Alg 700 °C showed an incremental change in pH values as a function of time (days) as shown in Fig. 3a, and the major change was observed within 6 days after which the pH remains constant. The 1% BM–Alg showed higher pH values than 70S30C BM because of the higher surface area which leads to faster ion exchange between the composite surface and SBF solution. Whereas, the 1% BM–Alg 700 °C demonstrated more pH values because of the porous nature produced due to the decomposition of the Alg. The change in pH values is indicative of the degradation rate of the sample. Thus, the degradation study of the synthesized samples was performed in SBF solution.

The degradation of the scaffold in host tissue is a requisite characteristic property that any composite should possess. The degradation rate is reliant on immersion time, molecular weight, crystallinity, and hydrophilicity.[30] Fig. 3b shows the degradation rate in terms of weight loss percentage for 70S30C BM, 1% BM–Alg, and 1% BM–Alg 700 °C after 3, 7, and 14 days of SBF immersion. The 70S30C BM displayed a 3.96% weight loss percentage, whereas, 1% BM–Alg and 1% BM–Alg 700 °C showed 58% and 22.6% weight loss percentage after 14 days. The 1% BM–Alg revealed more weight loss percentage than 1% BM–Alg 700 °C even though the porous nature of 1% BM–Alg 700 °C is more than 1% BM–Alg. This is because, during the

experiment, it was observed that after immersion of 1% BM–Alg composite in SBF solution, the pellet was converted into powder form (within 2 h) due to the breaking of bonds between BM, Alg, and $CaCl_2$, which leads to more weight loss. In addition, the differences in degradation percentage in the present study make manifold choices in the regeneration field because in gene delivery fast-degraded composites were used; whereas, in nerve regeneration, the composites having a moderate degradation rate are preferred.[8] In addition, during bone regeneration, the synthesized material should degrade at a rate corresponding with rate of bone formation to maintain the stability of bone and implanted material and allow the bone to grow.

Further, the growth of HAp on the composite surface was analyzed by XRD, FTIR, and SEM analysis. Fig. 3c displays the XRD pattern for 70S30C BM, 1% BM–Alg, and 1% BM–Alg 700 °C composite after 14 days of SBF study. The XRD pattern for 70S30C BM, 1% BM–Alg, and 1% BM–Alg 700 °C displayed reflection planes at (200), (111), (002), (210), (112), (202), (212), (221), (113), (320), (213), (402), and (004) characteristic of HAp (JCPDS no: 09-0432). It was observed that 1% BM–Alg showed intense peaks for HAp as compared with 1% BM–Alg 700 °C. The HAp formation on 1% BM–Alg and 1% BM–Alg 700 °C surface was further analyzed by FTIR analysis. The newly observed peaks for Si–OH were detected at $\sim$565 and $\sim$894 cm^{-1} after an exchange of H$^+$ ions with Na$^+$ and H$^+$. Then the carbonate (CO_3^{2-}) groups were attracted and showed C–O stretching frequency at $\sim$1422 cm^{-1}. Finally, the phosphate groups were adsorbed on the carbonate group leading to HAp formation. The peaks for the phosphate group were detected at $\sim$642, $\sim$1014, and $\sim$1086 cm^{-1}.[6] Thus, FTIR data revealed the growth of HAp on the sample surface. To support the XRD and
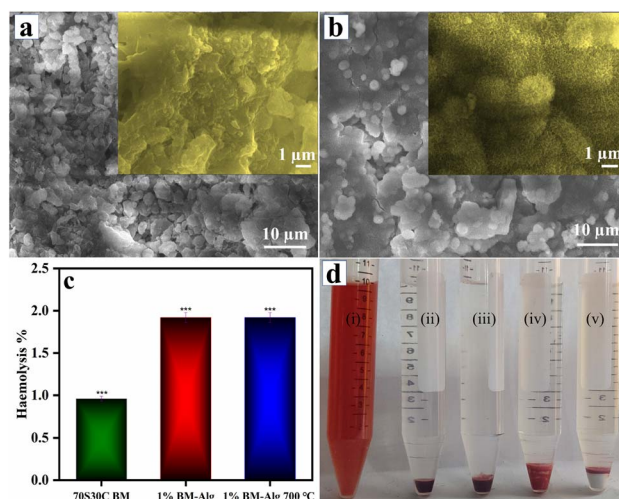

Fig. 4 SEM images of (a) 1% BM–Alg and (b) 1% BM–Alg 700 °C (inset showed magnified images) after 14 days of SBF immersion. (c) *In vitro* haemocompatibility assay using human blood (d) Suspension solution of (i) positive control, (ii) negative control, (iii) 70S30C BM, (iv) 1% BM–Alg, and (v) 1% BM–Alg 700 °C ($n = 3$) $p < 0.05$ at *$p \leq 0.05$, **$p \leq 0.01$, ***$p \leq 0.001$ by one-way analysis of variance (ANOVA) with Dunnet comparison test.
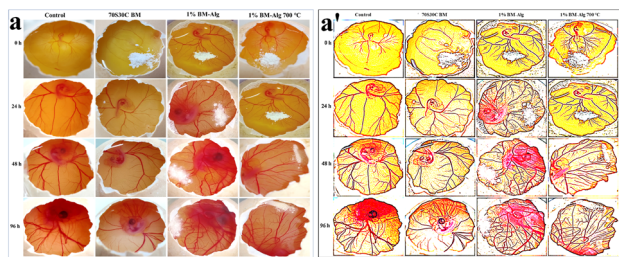
Fig. 5 (a) Angiogenesis study of 70S30C BM, 1% BM–Alg, and 1% BM–Alg 700 °C composite as a function of time (0, 24, 48 and 96 h) (*n* = 3). (a′) Corresponding images obtained after processing the images using ImageJ software (Mexican Hat Filter) for clarity of presentation.

FTIR data, the actual morphological changes on the surface were observed by SEM analysis.

Fig. 4a demonstrates the SEM images for 1% BM–Alg and 1% BM–Alg 700 °C composite after 14 days of immersion in SBF solution. The 1% BM–Alg and 1% BM–Alg 700 °C revealed the formation of globular HAp after 14 days of the SBF study. The magnified image as shown in Fig. 4a inset for 1% BM–Alg displayed the dense nature of HAp formation due to the hydrophilic nature of Alg, whereas, the magnified image of 1% BM–Alg 700 °C displayed a porous nature because calcination creates more pores for ion exchange (Fig. 4b inset). The 1% BM–Alg images matched very well with the results reported by Srinivasan *et al.* study for alginate/nano BG-ceramic composite.[33] Thus, the changes observed in SEM images before and after immersion in SBF reveal the growth of HAp on the synthesized samples. Further, the haemocompatibility of the 70S30C BM, 1% BM–Alg, and 1% BM–Alg 700 °C samples were examined.

A haemolysis study was performed because if the sample is considered as an implant material, it ultimately comes in contact with blood and thus it is recommended to follow ASTM 756-00 and ISO 10 993-51,992.[8] If the samples possess less than 5% haemolysis, it is considered as hemocompatible. Fig. 4c demonstrates that the haemolysis percentage of 70S30C BM, 1% BM–Alg, and 1% BM–Alg 700 °C is 0.96 ± 0.057, 1.92 ± 0.035, and 1.92 ± 0.040, respectively. In addition, after the completion of haemolysis experiments, the images were captured as shown in Fig. 4d. Fig. 4d showed images of positive control, negative control, 70S30C BM, 1% BM–Alg, and 1% BM–Alg 700 °C. The positive control is the ruptured blood cells, whereas, a negative control is demonstrated for unruptured blood cells. The sample images were compared with negative control and all the samples showed unruptured blood cells, which revealed its haemocompatibility. A haemocompatibility study of Alg, nBG-Alg, and nBG-Zr/Alg hydrogels reported by Bargavi *et al.* showed <1% haemolysis.[8] Further, the angiogenesis study was performed on the *ex ovo* CAM model.

Angiogenesis is the formation of the blood vessels that help to transport nutrients and ions during the bone healing process. Thus, the CAM study was performed to study the angiogenic nature of the synthesized samples. The 70S30C BM, 1% BM–Alg, and 1% BM–Alg 700 °C demonstrated the formation and growth of the new blood vessels with time (24, 48, and
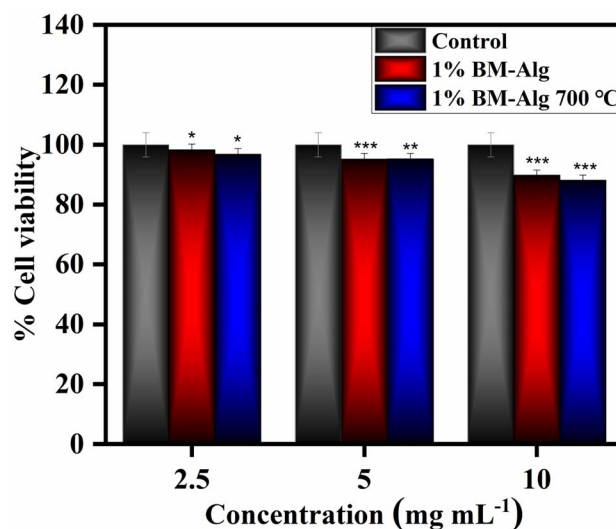

Fig. 6 Percentage cell viability of 70S30C, 1% BM–Alg, and 1% BM–Alg 700 °C at 2.5, 5, and 10 mg mL^{-1} using MG-63 bone cells (*n* = 3) *p* < 0.05 at *$p \leq 0.05$, **$p \leq 0.01$, ***$p \leq 0.001$ by one-way analysis of variance (ANOVA) with Dunnet comparison test.

96 h) without sign of toxic effect as shown in Fig. 5. To support the angiogenesis, the biocompatibility study, which means brine shrimp lethality and MTT assay was also performed.

The brine shrimp lethality assay is employed to assess the toxicity of a synthesized sample by exposing it to shrimp larvae. This method serves as an initial analysis for toxicity testing. The toxicity evaluation for 1% BM–Alg and 1% BM–Alg 700 °C samples is shown in Table S1.† As shown in Table S1,† there is no notable mortality observed for the samples at 10, 100, and 1000 μg concentrations and it showed a marginal increase with the increase in concentration. These findings are further verified by a cell viability assay conducted using MG-63 cells.

Fig. 6 shows *in vitro* biocompatibility results for 1% BM–Alg and 1% BM–Alg 700 °C composite. The 2.5–10 mg mL^{-1} sample concentrations were used to detect the percentage cell viability of the samples. The 1% BM–Alg and 1% BM–Alg 700 °C display 98.30 ± 0.977, 95.21 ± 0.898, 89.78 ± 0.455, and 96.81 ± 1.546, 95.25 ± 1.911, and 88.12 ± 0.496 percentage cell viability at 2.5, 5, and 10 mg mL^{-1} concentrations after 24 h. The 1% BM–Alg and 1% BM–Alg 700 °C demonstrate more than 70% cell viability revealing a non-toxic nature according to the International Organization for Standardization (ISO) 10993-5.[23] Thus, the present study reveals that 1% BM–Alg and 1% BM–Alg 700 °C composite show a non-toxic nature. Further, the study was supported by checking the *in vivo* biocompatibility results.

The *in vivo* biocompatibility study was investigated for 1% BM–Alg and 1% BM–Alg 700 °C, through subcutaneous implantation in rat skin pockets as shown in Fig. 7a and b. After 14 days, the surgery was reopened and biocompatibility was checked by taking photographic images (Fig. 7c and d). It was seen that, the 1% BM–Alg and 1% BM–Alg 700 °C composite pellet completely degraded without causing inflammation or adverse effects. Further, it was supported with the histological analysis, and the H&E-stained images of 1% BM–Alg and 1%
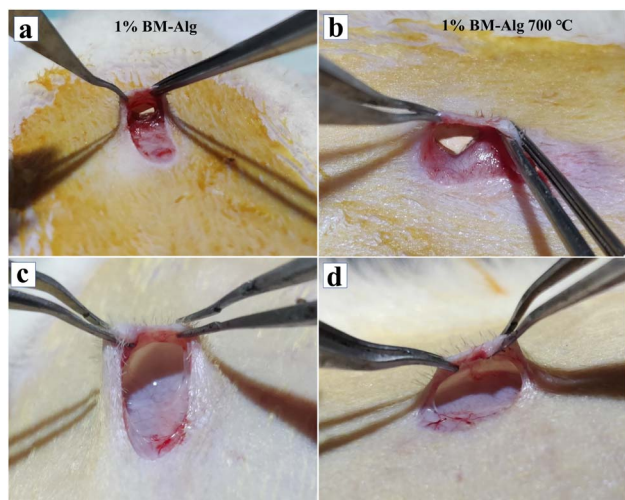
Fig. 7 *In vivo* biocompatibility study. Photographs of (a) 1% BM–Alg and (b) 1% BM–Alg 700 °C sample during the implantation and (c) 1% BM–Alg and (d) 1% BM–Alg 700 °C after 14 days of implantation, respectively ($n = 3$).
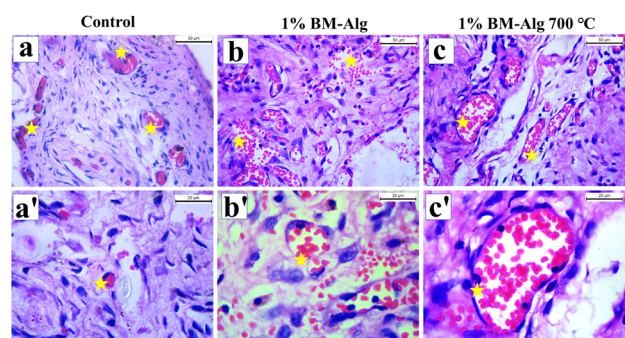

Fig. 8 Histological images of (a) and (a′) control (normal skin tissue); (b) and (b′) 1% BM–Alg; and (c) and (c′) 1% BM–Alg 700 °C. The figure shows endothelial cells having blood cells (highlighted by a star mark).

BM–Alg 700 °C were compared with the control as shown in Fig. 8a–c′. All samples exhibited the presence of endothelial cells containing blood cells indicating a positive tissue response. The findings highlight the favorable *in vivo* biocompatibility of both composites showing promise in fostering neovascularization for the regeneration of large bone defects.

4.   Conclusion

The porous and biocompatible composite was synthesized using BM and Alg through simple cross-linking. Primarily, the BM was prepared by rice husk and eggshell as a source of silica and calcium. The BET results suggested 275.79, 62.35, and 27.36 $m^2\ g^{-1}$ surface area for 1%, 3%, and 5% BM–Alg composite having mesoporous nature. The porosity of the 1% BM–Alg was found to increase after calcination (700 °C) due to the decomposition of Alg in the composite, which enhanced its porous nature. The synthesized materials were characterized by XRD, FTIR, and SEM analysis. The *in vitro* bioactivity results

showed growth of HAp formation on the 1% BM–Alg and 1% BM–Alg 700 °C surface. In addition, the 1% BM–Alg and 1% BM–Alg 700 °C showed 58% and 22.6% weight loss percentage after 14 days. Further, the *in vitro* haemolysis results demonstrate less than 5% haemolysis which revealed the haemocompatibility of the samples. The *ex ovo* CAM assay was performed and the result revealed the growth and development of blood vessels without adverse effects. The *in vitro* biocompatibility results on MG-63 cells showed a non-toxic nature at 2.5–10 mg mL^{-1} concentration. Further, outcomes from the *in vivo* biocompatibility assessment demonstrate the non-toxic nature of the material even after 14 days of subcutaneous study. Thus, the present work serves as a cost-effective, eco-friendly, acid-free, and binder-free approach and the 1% BM–Alg and 1% BM–Alg 700 °C composite demonstrated its applicability towards bone regeneration along with drug delivery and nerve regeneration.

Ethical statement

The methodology for this study was approved by the Institutional Animal Ethics Committee approval of the University of D. Y. Patil Medical College Kolhapur (Approval No. 6/IAEC/2017).

Data availability

The data will be made available from the corresponding author upon reasonable request.

Author contributions

Shital S. Shendage: conceptualization, methodology, design experiment, investigation, data collection, data curation, writing the original draft. Kranti Kachare: synthesis, data curation, writing, and review. Kajal Gaikwad: angiogenesis, antibacterial, haemolysis, and *in vivo* study. Shivaji Kashte: biological assays, guidelines for execution, data curation, writing, review, and editing. Anil Vithal Ghule: conceptualization of the project, planning of the experiments, guidelines for execution of the project, following the investigation, methodology, data curation, interpretation, supervision, validation, drafting of the manuscript, review, editing, and finalizing the draft.

Conflicts of interest

There are no conflicts to declare.

Acknowledgements

References

1 R. R. Sehgal, E. Carvalho and R. Banerjee, Mechanically Stiff, Zinc Cross-Linked Nanocomposite Scaffolds with Improved Osteostimulation and Antibacterial Properties, *ACS Appl. Mater. Interfaces*, 2016, **8**(22), 13735–13747, DOI: **10.1021/acsami.6b02740**.

2 S. Pant, S. Thomas, S. Loganathan and R. B. Valapa, 3D Bioprinted Poly(Lactic Acid)/Mesoporous Bioactive Glass Based Biomimetic Scaffold with Rapid Apatite Crystallization and In-Vitro Cytocompatability for Bone Tissue Engineering, *Int. J. Biol. Macromol.*, 2022, **217**(July), 979–997, DOI: **10.1016/j.ijbiomac.2022.07.202**.

3 G. Luo, Y. Ma, X. Cui, L. Jiang, M. Wu, Y. Hu, Y. Luo, H. Pan and C. Ruan, 13-93 Bioactive Glass/Alginate Composite Scaffolds 3D Printed under Mild Conditions for Bone Regeneration, *RSC Adv.*, 2017, **7**(20), 11880–11889, DOI: **10.1039/c6ra27669e**.

4 S. Jadbabaei and M. Kolahdoozan, Preparation and Characterization of Sodium Alginate – PVA Polymeric Sca Ff Olds by Electrospinning Method for Skin Tissue Engineering, *RSC Adv.*, 2021, **11**, 30674–30688, DOI: **10.1039/d1ra04176b**.

5 S. D. Purohit, R. Bhaskar, H. Singh, I. Yadav, M. K. Gupta and N. C. Mishra, Development of a Nanocomposite Scaffold of Gelatin–Alginate–Graphene Oxide for Bone Tissue Engineering, *Int. J. Biol. Macromol.*, 2019, **133**, 592–602, DOI: **10.1016/j.ijbiomac.2019.04.113**.

6 A. C. Özarslan, Y. B. Elalmis and S. Yücel, Production of Biosilica Based Bioactive Glass-Alginate Composite Putty as Bone Support Material, and Evaluation of In Vitro Properties; Bioactivity and Cytotoxicity Behavior, *J. Non-Cryst. Solids*, 2021, **561**, 120755, DOI: **10.1016/j.jnoncrysol.2021.120755**.

7 F. Zhao, W. Zhang, X. Fu, W. Xie and X. Chen, Fabrication and Characterization of Bioactive Glass/Alginate Composite Sca Ff Olds by a Self-Crosslinking Processing for Bone Regeneration, *RSC Adv.*, 2016, **6**, 91201–91208, DOI: **10.1039/C6RA18309C**.

8 P. Bargavi, R. Ramya, S. Chitra, S. Vijayakumari, R. Riju Chandran, D. Durgalakshmi, P. Rajashree and S. Balakumar, Bioactive, Degradable and Multi-Functional Three-Dimensional Membranous Scaffolds of Bioglass and Alginate Composites for Tissue Regenerative Applications, *Biomater. Sci.*, 2020, **8**(14), 4003–4025, DOI: **10.1039/d0bm00714e**.

9 J. S. Fernandes, P. Gentile, R. A. Pires, R. L. Reis and P. V. Hatton, Multifunctional Bioactive Glass and Glass-Ceramic Biomaterials with Antibacterial Properties for Repair and Regeneration of Bone Tissue, *Acta Biomater.*, 2017, **59**, 2–11, DOI: **10.1016/j.actbio.2017.06.046**.

10 S. Liu, W. Gong, Y. Dong, Q. Hu, X. Chen and X. Gao, The Effect of Submicron Bioactive Glass Particles on in Vitro Osteogenesis, *RSC Adv.*, 2015, **5**(49), 38830–38836, DOI: **10.1039/c5ra03786g**.

11 F. Zhao, W. Zhang, X. Fu, W. Xie and X. Chen, Fabrication and Characterization of Bioactive Glass/Alginate Composite Scaffolds by a Self-Crosslinking Processing for Bone Regeneration, *RSC Adv.*, 2016, **6**(94), 91201–91208, DOI: **10.1039/c6ra18309c**.

12 A. Hoppe, B. Jokic, D. Janackovic, T. Fey, P. Greil, S. Romeis, J. Schmidt, W. Peukert, J. Lao, E. Jallot and A. R. Boccaccini, Cobalt-Releasing 1393 Bioactive Glass-Derived Scaffolds for Bone Tissue Engineering Applications, *ACS Appl. Mater. Interfaces*, 2014, **6**(4), 2865–2877, DOI: **10.1021/am405354y**.

13 Y. Efraim, B. Schoen, S. Zahran, T. Davidov, G. Vasilyev, L. Baruch, E. Zussman and M. Machluf, 3D Structure and Processing Methods Direct the Biological Attributes of ECM-Based Cardiac Scaffolds, *Sci. Rep.*, 2019, **9**(1), 1–13, DOI: **10.1038/s41598-019-41831-9**.

14 Y. Ding, W. Li, A. Correia, Y. Yang, K. Zheng, D. Liu, D. W. Schubert, A. R. Boccaccini, H. A. Santos and J. A. Roether, Electrospun Polyhydroxybutyrate/Poly(ε-Caprolactone)/Sol-Gel-Derived Silica Hybrid Scaffolds with Drug Releasing Function for Bone Tissue Engineering Applications, *ACS Appl. Mater. Interfaces*, 2018, **10**(17), 14540–14548, DOI: **10.1021/acsami.8b02656**.

15 A. Haider, A. Waseem, N. Karpukhina and S. Mohsin, Strontium-and Zinc-Containing Bioactive Glass and Alginates Scaffolds, *Bioengineering*, 2020, **7**(10), 1–17, DOI: **10.3390/bioengineering7010010**.

16 J. Hatton, G. R. Davis, A. H. I. Mourad, N. Cherupurakal, R. G. Hill and S. Mohsin, Fabrication of Porous Bone Scaffolds Using Alginate and Bioactive Glass, *J. Funct. Biomater.*, 2019, **10**(1), 1–14, DOI: **10.3390/jfb10010015**.

17 S. Fu, X. Du, M. Zhu, Z. Tian, D. Wei and Y. Zhu, 3D Printing of Layered Mesoporous Bioactive Glass/Sodium Alginate-Sodium Alginate Scaffolds with Controllable Dual-Drug Release Behaviors, *Biomed. Mater.*, 2019, **14**, 065011, DOI: **10.1088/1748-605X/ab4166**.

18 E. Babaie and S. B. Bhaduri, Fabrication Aspects of Porous Biomaterials in Orthopedic Applications: A Review, *ACS Biomater. Sci. Eng.*, 2018, **4**(1), 1–39, DOI: **10.1021/acsbiomaterials.7b00615**.

19 A. Cianciosi, M. Costantini, S. Bergamasco, S. Testa, E. Fornetti, J. Jaroszewicz, J. Baldi, A. Latini, E. Choińska, M. Heljak, C. Zoccali, S. Cannata, W. Święszkowski, A. Diaz Lantada, C. Gargioli and A. Barbetta, Engineering Human-Scale Artificial Bone Grafts for Treating Critical-Size Bone Defects, *ACS Appl. Bio Mater.*, 2019, **2**(11), 5077–5092, DOI: **10.1021/acsabm.9b00756**.

20 T. Kokubo and S. Ito, Ca, P-Rich Layer Formed on High-Strength Bioactive Glass-Ceramic A-W, *J. Biomed. Mater. Res.*, 1990, **24**(3), 331–343, DOI: **10.1002/jbm.820240306**.

21 S. S. Shendage, V. H. Ingole, A. Rasal, J. Y. Chang, N. B. Birajdar, A. P. Tiwari, S. Kashte, T. Vuherer, G. Schmitt, M. Cucchiarini and A. V. Ghule, Sustainable Development of a Bioactive Material from Recycled Rice Husk and Eggshell for Bone Regeneration Application, *ACS*

Sustainable Chem. Eng., 2024, **12**, 2598–2610, DOI: **10.1021/acssuschemeng.3c06290**.

22 B. N. Meyer, N. R. Ferrigni, J. E. Putnam, L. B. Jacobsen, D. E. Nichols and J. L. McLaughlin, Brine Shrimp: A Convenient General Bioassay for Active Plant Constituents, *Planta Med.*, 1982, **45**(1), 31–34, DOI: **10.1055/s-2007-971236**.

23 S. S. Shendage, K. Gaikwad, K. Kachare, S. Kashte and A. V. Ghule, In Vitro and In Vivo Study of Copper-Doped Bioactive Glass for Bone Regeneration Application, *Mater. Chem. Phys.*, 2024, **313**, 128789, DOI: **10.1016/j.matchemphys.2023.128789**.

24 H. P. Felgueiras and M. T. P. Amorim, *Production of Polymer–Bioactive Glass Nanocomposites for Bone Repair and Substitution*, Elsevier Inc., 2019, DOI: **10.1016/b978-0-12-816909-4.00012-9**.

25 J. Xiao, Q. Wei, J. Xue, Z. Liu, Z. Li, Z. Zhou, F. Chen and F. Zhao, Mesoporous Bioactive Glass/Bacterial Cellulose Composite Scaffolds for Bone Support Materials, *Colloids Surf., A*, 2022, **642**(January), 128693, DOI: **10.1016/j.colsurfa.2022.128693**.

26 M. S. Ur Rahman, M. A. Tahir, S. Noreen, M. Yasir, I. Ahmad, M. B. Khan, K. W. Ali, M. Shoaib, A. Bahadur and S. Iqbal, Magnetic Mesoporous Bioactive Glass for Synergetic Use in Bone Regeneration, Hyperthermia Treatment, and Controlled Drug Delivery, *RSC Adv.*, 2020, **10**(36), 21413–21419, DOI: **10.1039/c9ra09349d**.

27 H. Türe, Development of Copper-Doped Bioglass/Alginate Composite Membranes : Preliminary Results on Their Characterization and Antimicrobial Properties, *Mater. Today Commun.*, 2019, (July), 100583, DOI: **10.1016/j.mtcomm.2019.100583**.

28 R. Wetzel, M. Blochberger, F. Scheffler, L. Hupa and D. S. Brauer, Mg or Zn for Ca Substitution Improves the Sintering of Bioglass 45S5, *Sci. Rep.*, 2020, **10**, 15964, DOI: **10.1038/s41598-020-72091-7**.

29 J. V. Rau, M. Curcio, M. G. Raucci, K. Barbaro, I. Fasolino, R. Teghil, L. Ambrosio, A. De Bonis and A. R. Boccaccini, Cu-Releasing Bioactive Glass Coatings and Their In Vitro Properties, *ACS Appl. Mater. Interfaces*, 2019, **11**(6), 5812–5820, DOI: **10.1021/acsami.8b19082**.

30 D. Zamani, F. Moztarzadeh and D. Bizari, Alginate-Bioactive Glass Containing Zn and Mg Composite Scaffolds for Bone Tissue Engineering, *Int. J. Biol. Macromol.*, 2019, **137**, 1256–1267, DOI: **10.1016/j.ijbiomac.2019.06.182**.

31 J. Wu, S. Wang, Z. Zheng and J. Li, Fabrication of Biologically Inspired Electrospun Collagen/Silk Fibroin/Bioactive Glass Composited Nano Fibrous Scaffold to Accelerate the Treatment Efficiency of Bone Repair, *Regener. Ther.*, 2022, **21**, 122–138, DOI: **10.1016/j.reth.2022.05.006**.

32 M. D. Esposti, M. Changizi, R. Salvatori, L. Chiarini, V. Cannillo, D. Morselli and P. Fabbri, Comparative Study on Bioactive Filler/Biopolymer Scaffolds for Potential Application in Supporting Bone Tissue Regeneration, *ACS Appl. Polym. Mater.*, 2022, **4**(6), 4306–4318, DOI: **10.1021/acsapm.2c00270**.

33 S. Srinivasan, R. Jayasree, K. P. Chennazhi, S. V. Nair and R. Jayakumar, Biocompatible Alginate/Nano Bioactive Glass Ceramic Composite Scaffolds for Periodontal Tissue Regeneration, *Carbohydr. Polym.*, 2012, **87**(1), 274–283, DOI: **10.1016/j.carbpol.2011.07.058**.